A New Phase-Equilibrium Model for Simulating Industrial Nylon-6 Production Trains

Kevin C. Seavey, Neeraj P. Khare, and Y. A. Liu*

Honeywell Center of Excellence in Computer-Aided Design, Department of Chemical Engineering, Virginia Polytechnic Institute and State University, Blacksburg, Virginia 24061

Thomas N. Williams

Honeywell International, Inc., 15801 Woods Edge Road, Colonial Heights, Virginia 23834

Chau-Chyun Chen

Aspen Technology, Inc., Ten Canal Park, Cambridge, Massachusetts 02141

This paper presents a thermodynamically consistent model for the phase equilibrium of water/caprolactam/nylon-6 mixtures, based on the POLYNRTL (polymer nonrandom two-liquid) activity-coefficient model. Our model predicts phase equilibrium for any binary or ternary mixture containing water, ϵ-caprolactam, and nylon-6 at industrially relevant temperatures and pressures with an average error of 1%. This paper also demonstrates its application to simulate a melt train and a bubble-gas kettle train for industrial production of nylon-6. Prior literature makes simplifying assumptions about liquid-phase (molten polymer) activities of water and ϵ-caprolactam; these assumptions are shown to be unrealistic.

1. Introduction

It is hard to overestimate the importance of nylon in the development of polymer science and in the commercial growth of polymer applications. Nylon was discovered by Wallace Hume Carothers in 1935 and produced commercially by DuPont and IG Farben beginning in 1939.[1] Nylon's combination of strength, toughness, and high melt temperature made it the first engineering thermoplastic, capable of myriad uses. It quickly found application in synthetic fibers, which continue to dominate its current production of 12.5 billion lbs/year.[2,3] Other high- volume applications include household articles, automotive parts, electrical cable, and packaging.

There are two major types of nylon: (1) nylon-6,6 made commercially by the condensation polymerization of adipic acid with hexamethylenediamine; (2) nylon-6, made from the ring opening of ϵ-caprolactam and its subsequent polycondensation. While nylon-6,6 dominates production in the U.S., nylon-6 is dominant in Europe and Asia. Nylon-6 production accounts for approximately 7 billion lbs/year of fibers and resins.

Considering the economic scale of nylon-6 production, it is not surprising that a number of polymerization models based on first principles have appeared.[4−8] These models attempt to apply knowledge of kinetics, physical and thermodynamic properties, mass and energy transport, and phase equilibrium to simulate a manufacturing process. We can apply an accurate model to improve the product quality, increase the production rate, and reduce production costs.

This paper addresses inaccuracies in phase equilibrium that limit the accuracy of these existing models. In particular, we describe commercial nylon-6 manufacturing technologies to demonstrate the critical impact of phase equilibrium. We then outline prior simulation studies that seek to understand and optimize these processes and their deficiencies. Lastly, we discuss current problems facing the simulation of nylon-6 phase equilibrium and show how to address these problems.

1.1. Commercial Nylon-6 Manufacturing Processes. Figure 1 depicts a conventional nylon-6 production scheme.

The reactor feed typically contains fresh caprolactam monomer, recycled monomer, water, and desired additives,[9] such as chain-terminating agents, fire-retarding agents, and delustrants. The reactor section hydrolyzes the monomer, converts it to a polymer, and builds up the polymer molecular weight.

Because the molten polymer is in equilibrium with water and monomer, the byproduct water must be removed by vaporization to increase the molecular weight. However, vaporization of the water may also remove a significant amount of caprolactam, which is recovered and recycled.

In conventional processes, the polymer is then pelletized and leached with hot water to remove low-molecular-weight extractables, such as residual monomer and cyclic oligomers. The polymer is then dried and shipped elsewhere or used directly to spin fibers.[10]

By contrast, in direct melt processes, the extraction and drying steps are avoided by devolatilizing the polymer of unreacted monomer. Molten polymer can then be fed directly to spinning or pelletizing. However, melt polymers are typically modified (terminated with monofunctional amines and carboxylic acids) to limit the molecular weight produced at the low levels of water achieved when removing unreacted caprolactam. Therefore, direct melt processes have a limited product range compared with conventional processes.

Within these two process variants, i.e., conventional and direct melt, a number of commercial technologies

* To whom correspondence should be addressed. Tel.: (540) 231-7800. Fax: (540) 231-5022. E-mail: design@vt.edu.

10.1021/ie030112+ CCC: $25.00
Published on Web 07/18/2003

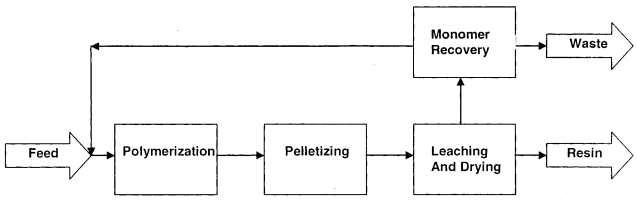

Figure 1. Block diagram of a conventional nylon-6 polymerization process.

Table 1. Nylon-6 Production−Recycling Technologies Practiced on a Commercial Scale and Their Associated Operating Conditions

industrial process	temperature (K)/pressure (kPa) range	ref
batch−semibatch	533/101.325−490.332	8, 12
bubble-gas kettle	528/101.325	13
VK column	517−555/101.325	5
melt process	473−573/0.67−648	10
solid state	383−478/101.325	14
depolymerization	513−673/10−1400	15

are available to polymerize caprolactam. These technologies include batch, bubble-gas kettle, melt (terminated and unterminated resins), traditional VK (Vereinfacht Kontinuierliches), and solid-state processes. Even the depolymerization of nylon-6 to recover caprolactam is practiced on a commercial scale.[11] Table 1 summarizes these major technologies along with their approximate temperature and pressure conditions.

The temperature for industrial nylon processes ranges from 383 to 673 K (110−400 °C). The pressure ranges from 0.67 to 1400 kPa (0.007−13.8 atm). This strikingly wide range of processing conditions underscores the need for a fundamental phase-equilibrium model that adequately represents all of these processes throughout the entire temperature and pressure ranges.

1.2. Previous Nylon-6 Process Simulation Research. We can better understand chemical manufacturing operations by developing simulation models that are based on the underlying engineering fundamentals. These simulation models can be used in a variety of beneficial ways: they speed up process development and optimization and can facilitate new product development.

Researchers who recognized the value of simulation began publishing models of nylon-6 polymerization in the 1970s, with Giori and Hayes[4] among the first. Initial models for most commercial nylon polymerization technologies have now been documented, including VK tube,[5] plug-flow,[6] wiped-film,[7] and semibatch reactors.[8]

In the modeling of any multiphase chemical manufacturing process, it is important to properly model the phase equilibrium of the process.[16] Specifically, we must pay particular attention to phase equilibrium when modeling nylon polymerizations. This is because the water concentration in the liquid phase is the overwhelming factor in determining product characteristics, such as the production rate and molecular weight.[8] Furthermore, properly representing the thermodynamics is the basis for fundamentally modeling mass-transfer resistances in step-growth finishing reactors. If we cannot adequately model phase equilibrium, then we will not be able to properly diagnose the appearance of significant mass-transfer limitations or calculate interfacial equilibrium compositions.

While it is clear that properly modeling the phase equilibrium in nylon polymerizations is important, it is unfortunate that virtually no nylon-6 model in the literature contains an accurate, fundamental thermodynamic model. This is because there is considerable uncertainty in the phase-equilibrium data themselves.[8] A possible exception is the modeling study by Loth et al.;[17] however, they give no details regarding their phase-equilibrium model.

Experimental phase-equilibrium measurements are difficult to make because the water/caprolactam/nylon-6 system is reactive. Furthermore, the mixture water/caprolactam is wide-boiling, with the normal boiling point of caprolactam above 260 °C. Characterizing this system and analyzing the resulting data require a deep understanding of the underlying kinetics and thermodynamics.

In an ideal world, we would have many sets of thermodynamically consistent phase-equilibrium data for water/caprolactam, water/nylon-6, and caprolactam/nylon-6. These data would cover a wide range of temperatures and pressures. Unfortunately, we suffer from a lack of data, and the literature data that we do have are inconsistent.

1.3. Objectives of the Current Study. We develop a thermodynamically consistent model for nylon-6 phase equilibrium using the appropriate information out of scarce and inconsistent literature data. This development involves characterizing the binary interactions between caprolactam, water, and nylon-6.

This fundamental model represents an important advance in the ability to simulate nylon-6 polymerizations because it facilitates *integrated process modeling*. When we perform integrated process modeling, we build unified models of entire manufacturing trains, not just reactors. In nylon-6 integrated process modeling, we simulate reactors, flash units, and condensers, all of which together cover wide ranges of pressures and temperatures.

We rely entirely on literature data to develop the present model. First, we demonstrate that the available data for water/caprolactam are thermodynamically inconsistent, and then we use only the temperature−pressure−liquid-mole-fraction ($T-P-x$) data to regress binary interaction parameters for water/caprolactam. Then, by simulating the reactive system, water/caprolactam/nylon-6, we are able to extract binary interaction parameters for water/nylon-6 and caprolactam/nylon-6 segments.

We then validate our phase-equilibrium model by comparing its predictions with plant experience for a condenser and two finishing reactors. Lastly, we demonstrate the utility of our thermodynamic model by developing integrated process simulations for a melt train and a bubble-gas kettle train for industrial nylon-6 production.

2. Literature Review

We split our literature review into three sections: nylon-6 polymerization kinetics, phase-equilibrium modeling, and water/caprolactam/nylon-6 phase-equilibrium data from the literature. We report nylon-6 polymerization kinetics for two reasons. First, we simulate the reactive system to obtain the binary interaction parameters for water/nylon-6 and caprolactam/nylon-6 segments. Second, we use the existing kinetic model, along with our thermodynamic and mass-transfer models, to build integrated models for commercial nylon-6 processes.

Table 2. Nylon-6 Hydrolytic Polymerization Reaction Mechanisms[a]

reaction name	equilibrium reaction
ring opening of caprolactam	$W + CL \underset{k_1'}{\overset{k_1}{\rightleftharpoons}} P_1$
polycondensation	$P_m + P_n \underset{k_2'}{\overset{k_2}{\rightleftharpoons}} P_{m+n} + W$
polyaddition of caprolactam	$CL + P_n \underset{k_3'}{\overset{k_3}{\rightleftharpoons}} P_{n+1}$
ring opening of cyclic dimer	$W + CD \underset{k_4'}{\overset{k_4}{\rightleftharpoons}} P_2$
polyaddition of cyclic dimer	$CD + P_n \underset{k_5'}{\overset{k_5}{\rightleftharpoons}} P_{n+2}$

[a] P_1 is aminocaproic acid. P_n is a nylon-6 molecule with a degree of polymerization n.

2.1. Nylon-6 Polymerization Kinetics. Arai et al.[18] have presented the accepted standard regarding the chemistry and kinetics of the hydrolytic polymerization of ϵ-caprolactam. Their reaction mechanism includes the ring opening of caprolactam (CL), polycondensation, polyaddition of CL, ring opening of a cyclic dimer (CD), and polyaddition of a CD. Table 2 lists these five equilibrium reactions.

Table 3 gives the accompanying rate constants k_i, again from Arai et al.[18]

We add one more equilibrium reaction to this kinetic scheme: the termination reaction with a monofunctional acid, such as acetic acid (AA).

$$AA + P_n \underset{k_2}{\overset{k_2'}{\rightleftharpoons}} P_{nx} + W \qquad (1)$$

We assume that this reaction follows the same kinetics as the polycondensation reaction, as in ref 5.

We ignore the analysis of cyclic oligomers higher than dimers for the sake of simplicity.

We use Aspen Technology's (Cambridge, MA) commercial simulation package POLYMERS PLUS to simulate nylon-6 polymerizations. This package implements the above reaction-kinetics model using the segment-based methodology detailed in the patent by Barrera et al.[19] This methodology tracks the polymer concentration and number-average degree of polymerization by tracking the concentrations of their constitutive segments. Figure 2 shows the segmental breakdown of nylon-6 molecules that can be either unterminated or terminated by AA.

Nylon-6 segments include the nylon-6 repeat segment (B-ACA) and the end groups terminal amine (T-NH_2), terminal carboxylic acid (T-COOH), and terminal AA (T-AA). Table 4 presents the reactions in Table 2 expressed using segment notation.

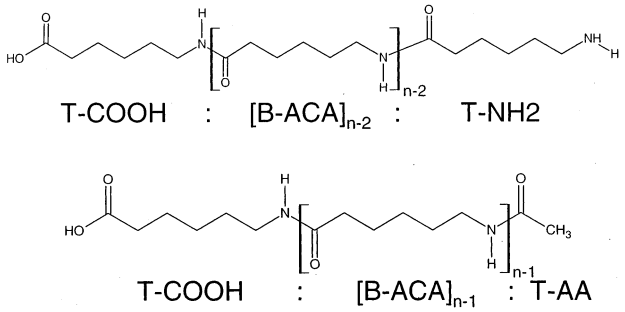

Figure 2. Nylon-6 molecules of degree of polymerization n existing as two types: unterminated (above) and terminated by AA (below). B-ACA represents nylon-6 repeat segments, T-NH_2 represents amine end groups, T-COOH represents carboxylic acid end groups, and T-AA represents AA end groups.

Table 4 also gives the associated reaction rates for each equilibrium reaction. Table 5 gives the species conservation equations corresponding to the reaction rates of Table 4.

POLYMERS PLUS estimates the concentrations of oligomers of degree of polymerization 2 and 3 below:

$$[P_2] = [\text{T-COOH}]\left(\frac{[\text{T-NH}_2]}{[\text{B-ACA}] + [\text{T-NH}_2]}\right) \qquad (2)$$

$$[P_3] = [\text{T-COOH}]\left(\frac{[\text{B-ACA}]}{[\text{B-ACA}] + [\text{T-NH}_2]}\right)\left(\frac{[\text{T-NH}_2]}{[\text{B-ACA}] + [\text{T-NH}_2]}\right) \qquad (3)$$

We compute the number-average degree of polymerization, DP_n, by considering the distribution of polymer chain lengths. This distribution contains m different chain lengths, with each chain length i characterized by a population of N_i chains with degree of polymerization DP_i:

$$DP_n = \frac{\sum_{i=1}^{m} N_i DP_i}{\sum_{i=1}^{m} DP_i} \qquad (4)$$

In terms of segments, the numerator of eq 4 represents the total concentration of segments that count as repeat units, or ([B-ACA] + [T-COOH] + [T-NH2] + [P_1]). The denominator represents the concentration of polymer

Table 3. Rate Constants for the Equilibrium Reactions in Table 2

rate constant expression	$k_i = A_i^0 \exp\left(-\frac{E_i^0}{RT}\right) + A_i^c \exp\left(-\frac{E_i^c}{RT}\right)[\text{T-COOH}]$
equilibrium constant expression	$K_i = \frac{k_i}{k_i'} = \exp\left(\frac{\Delta S_i - \Delta H_i/T}{R}\right)$

i	A_i^0 (kg/mol·s)	E_i^0 (J/mol)	A_i^c (kg^2/mol^2·s)	E_i^c (J/mol)	ΔH_i (J/mol)	ΔS_i (J/mol·K)
1	1.66×10^2	8.32×10^4	1.20×10^4	7.87×10^4	8.03×10^3	−33.01
2	5.26×10^6	9.74×10^4	3.37×10^6	8.65×10^4	-2.49×10^4	3.951
3	7.93×10^5	9.56×10^4	4.55×10^6	8.42×10^4	-1.69×10^4	−29.08
4	2.38×10^8	1.76×10^5	6.47×10^8	1.57×10^5	-4.02×10^4	−60.79
5	7.14×10^4	8.92×10^4	8.36×10^5	8.54×10^4	-1.33×10^4	2.439

Table 4. Nylon-6 Polymerization Reactions Written in Segment Notation[a]

equilibrium reaction	reaction rate
Ring-Opening of Caprolactam ($W + CL \underset{k_1'}{\overset{k_1}{\rightleftharpoons}} P_n$)	
$CL + W \underset{k_1'=k_1/K_1}{\overset{k_1}{\rightleftharpoons}} P_1$	$R_1 = k_1[CL][W] - k_1'[P_1]$
Polycondensation ($P_m + P_n \underset{k_2'}{\overset{k_2}{\rightleftharpoons}} P_{m+n} + W$)	
$P_1 + P_1 \underset{k_2'=k_2/K_2}{\overset{k_2}{\rightleftharpoons}}$ T-COOH:T-$NH_2 + W$	$R_2 = k_2[P_1]^2 - k_2'[P_2][W]$
$P_1 + $ T-COOH $\underset{k_2'=k_2/K_2}{\overset{k_2}{\rightleftharpoons}}$ T-COOH:B-ACA $+ W$	$R_3 = k_2[P_1][\text{T-COOH}] - k_2'[W][\text{T-COOH}]\left(\frac{[\text{B-ACA}]}{[\text{B-ACA}] + [\text{T-NH}_2]}\right)$
T-$NH_2 + P_1 \underset{k_2'=k_2/K_2}{\overset{k_2}{\rightleftharpoons}}$ T-NH_2:B-ACA $+ W$	$R_4 = k_2[\text{T-NH}_2][P_1] - k_2'[W][\text{T-NH}_2]\left(\frac{[\text{B-ACA}]}{[\text{B-ACA}] + [\text{T-COOH}]}\right)$
T-$NH_2 +$ T-COOH $\underset{k_2'=k_2/K_2}{\overset{k_2}{\rightleftharpoons}}$ B-ACA:B-ACA $+ W$	$R_5 = k_2[\text{T-NH}_2][\text{T-COOH}] - k_2'[W][\text{B-ACA}]\left(\frac{[\text{B-ACA}]}{[\text{B-ACA}] + [\text{T-NH}_2]}\right)$
Polyaddition of Caprolactam ($CL + P_n \underset{k_3'}{\overset{k_3}{\rightleftharpoons}} P_{n+1}$)	
$P_1 + CL \underset{k_3'=k_3/K_3}{\overset{k_3}{\rightleftharpoons}}$ T-NH_2:T-COOH	$R_6 = k_3[P_1][CL] - k_3'[P_2]$
T-$NH_2 + CL \underset{k_3'=k_3/K_3}{\overset{k_3}{\rightleftharpoons}}$ T-NH_2:B-ACA	$R_7 = k_3[\text{T-NH}_2][CL] - k_3'[\text{T-NH}_2]\left(\frac{[\text{B-ACA}]}{[\text{B-ACA}] + [\text{T-COOH}]}\right)$
Ring-Opening of Cyclic Dimer ($W + CD \underset{k_4'}{\overset{k_4}{\rightleftharpoons}} P_2$)	
$CD + W \underset{k_4'=k_4/K_4}{\overset{k_4}{\rightleftharpoons}}$ T-COOH:T-NH_2	$R_8 = k_4[CD][W] - k_4'[P_2]$
Polyaddition of Cyclic Dimer ($CD + P_n \underset{k_5'}{\overset{k_5}{\rightleftharpoons}} P_{n+2}$)	
$P_1 + CD \underset{k_5'=k_5/K_5}{\overset{k_5}{\rightleftharpoons}}$ T-NH_2:B-ACA:T-COOH	$R_9 = k_5[P_1][CD] - k_5'[P_3]$
T-$NH_2 + CD \underset{k_5'=k_5/K_5}{\overset{k_5}{\rightleftharpoons}}$ B-ACA:B-ACA:T-NH_2	$R_{10} = k_5[\text{T-NH}_2][CD] - k_5'[\text{T-NH}_2]\left(\frac{[\text{B-ACA}]}{[\text{B-ACA}] + [\text{T-COOH}]}\right)$
Polycondensation of Acetic Acid ($P_n + AA \underset{k_3'}{\overset{k_3}{\rightleftharpoons}} P_{n,\text{T-AA}}$)	
$P_1 + AA \underset{k_2'=k_2/K_2}{\overset{k_2}{\rightleftharpoons}}$ T-AA:T-COOH $+ W$	$R_{11} = k_2[AA][P_1] - k_2'[W][\text{T-AA}]\left(\frac{[\text{T-COOH}]}{[\text{T-COOH}] + [\text{B-ACA}]}\right)$
T-$NH_2 + AA \underset{k_2'=k_2/K_2}{\overset{k_2}{\rightleftharpoons}}$ B-ACA:T-AA $+ W$	$R_{12} = k_2[AA][\text{T-NH}_2] - k_2'[W][\text{T-AA}]\left(\frac{[\text{B-ACA}]}{[\text{T-COOH}] + [\text{B-ACA}]}\right)$

[a] A colon represents a covalent bond between segments.

Table 5. Species Conservation Equations for the Reaction Rates in Table 4

functional group	time rate of change
W	$d[W]/dt = R_2 + R_3 + R_4 + R_5 + R_{11} + R_{12} - (R_1 + R_8)$
CL	$d[CL]/dt = -(R_1 + R_6 + R_7)$
CD	$d[CD]/dt = -(R_8 + R_9 + R_{10})$
AA	$d[AA]/dt = -(R_{11} + R_{12})$
P_1	$d[P_1]/dt = R_1 - (2R_2 + R_3 + R_4 + R_6 + R_9 + R_{11})$
B-ACA	$d[\text{B-ACA}]/dt = R_3 + R_4 + 2R_5 + R_7 + R_9 + 2R_{10} + R_{12}$
T-NH_2	$d[\text{T-NH}_2]/dt = R_2 + R_6 + R_8 + R_9 - (R_5 + R_{12})$
T-COOH	$d[\text{T-COOH}]/dt = R_2 + R_6 + R_8 + R_9 + R_{11} - (R_5)$
T-AA	$d[\text{T-AA}]/dt = R_{11} + R_{12}$

chains, or ([T-COOH] + [P_1]). Therefore, we rewrite the number-average degree of polymerization below:

$$DP_n = \frac{[\text{B-ACA}] + [\text{T-NH}_2] + [\text{T-COOH}] + [P_1]}{[\text{T-COOH}] + [P_1]} \quad (5)$$

We do not compute the weight-average degree of polymerization, nor do we compute higher moments of the distribution of the DP.

2.2. Polymer Equilibrium. 2.2.1. Previous Attempts at Developing a Phase-Equilibrium Model for Water/Caprolactam/Nylon-6. Researchers typically use one of three phase-equilibrium models in simulating nylon-6 polymerizations: the Jacobs−Schweigman model,[20] the Fukumoto model,[21] or the Tai et al. model.[12] These models only predict water concentrations in reacting mixtures of water, caprolactam, and nylon-6.

The Jacobs−Schweigman model[20] is the most simplistic of the three models. It consists of an empiricism based on experimental equilibrium data for a VK (Vereinfacht Kontinuierliches) tube reactor. The model predicts the concentration of water [W] as a function of temperature T:

$$[W]\ (\text{mol/kg}) = \frac{1.76 - 0.006T\ (^\circ\text{C})}{1.8} \quad (6)$$

Table 6. Liquid-Phase, Water Mole-Fraction Predictions at 1 atm for the Jacobs−Schweigman,[20] Fukumoto,[21] and Tai et al.[12] Phase-Equilibrium Models

temp (K)	Jacobs−Schweigman	Fukumoto	Tai et al.
473	0.006	0.017	0.103
493	0.004	0.008	0.050
513	0.003	0.004	0.025
533	0.002	0.002	0.013

Because this expression does not contain pressure as a free variable and was developed using VK tube equilibrium data, it should not be used at pressures deviating from atmospheric pressure.

Adding the system pressure P to the Jacobs−Schweigman model results in the Fukumoto model[21] based on vapor−liquid equilibrium (VLE) data:

$$[\mathrm{W}]\ (\mathrm{mol/kg}) = P\ (\mathrm{mmHg})\ \exp\left(\frac{8220}{T\ (\mathrm{K})} - 24.0734\right) \quad (7)$$

The third model is the Tai et al. model,[12] which explicitly considers the partial pressures of volatile components. It consists of a system of three equations to solve for the mole fraction of water, x_W, given the temperature T and total pressure P:

$$\log\left[\frac{x_W}{P_W\ (\mathrm{mmHg})}\right] = \frac{3570}{T\ (\mathrm{K})} - 11.41 \quad (8)$$

$$\log[P_{CL}\ (\mathrm{mmHg})] = -\frac{4100}{T\ (\mathrm{K})} + 9.6 \quad (9)$$

$$P = P_W + P_{CL} \quad (10)$$

P_W is the partial pressure of water, and P_{CL} is the partial pressure of caprolactam.

All three models are empirical. Therefore, we cannot be confident in their phase-equilibrium predictions at conditions that deviate from those in which they are based.

Significantly, these three models give conflicting predictions for identical process conditions. Consider, for example, the water liquid-mole-fraction predictions at atmospheric pressure for a mixture of water, caprolactam, and nylon-6 at a range of relevant processing temperatures of 473−523 K (Table 6).

The Fukumoto model[21] predicts mole fractions that are about twice those of the Jacobs−Schweigman[20] predictions. Furthermore, the Tai et al. model[12] predicts mole fractions that are an order of magnitude higher than both models. This difference casts considerable doubt on the validity of at least two of these models.

2.2.2. Polymer Nonrandom Two-Liquid (POLYNRTL) Model. Bokis et al.[16] give an excellent description of how to choose an appropriate thermodynamic equilibrium model when simulating polymer processes. They suggest using activity-coefficient models, instead of equations of state, for processes that involve low-to-moderate pressures (pressure $< 1 \times 10^6$ Pa) and/or nonideal components (e.g., polar compounds such as alcohols, water, and ketones).

Furthermore, they state that the POLYNRTL activity-coefficient model[22] has the following advantages over the Flory−Huggins (FH)[23,24] and universal quasi-chemical functional group (UNIFAC)[25] activity-coefficient models:

1. POLYNRTL covers large ranges of temperatures and compositions accurately.

2. POLYNRTL takes advantage of the already existing database of NRTL binary interaction parameters.

On the basis of these suggestions, we choose to model nylon-6 phase equilibrium using the POLYNRTL property method. This method uses (1) the polymer NRTL activity-coefficient model for the liquid phases, (2) the Redlich−Kwong[26] equation of state for the vapor phase, (3) the van Krevelen[27] model for the liquid properties (enthalpy, entropy, Gibbs free energy, heat capacity, and molar volume), and (4) Henry's law for any supercritical components.

The POLYNRTL activity-coefficient model combines the traditional NRTL model with the FH description for configurational entropy. It essentially calculates the Gibbs free energy of mixing in a polymer solution as the sum of two contributions: (1) the entropy of mixing from the FH activity-coefficient model; (2) the enthalpy of mixing from the NRTL activity-coefficient model.[28] These activity coefficients include binary parameters to model the interactions between two components. POLYNRTL represents the temperature dependence of the binary interaction parameters (τ_{ij}) by eq 11. We set the

$$\tau_{ij} = a_{ij} + \frac{b_{ij}}{T} + c_{ij} \ln T \quad (11)$$

nonrandomness factor α_{ij} to 0.3, as suggested by Prausnitz et al.[29]

Therefore, we model binary interactions in equilibrium mixtures by specifying the coefficients a_{ij} through c_{ij}. We typically regress equilibrium data or use a predictive model, such as UNIFAC, to obtain the values of these parameters.

2.3. Equilibrium Data for Water/Caprolactam/Nylon-6. There are two sources of phase-equilibrium data that we use for regression. The first source characterizes the binary interactions between water and caprolactam. The second characterizes the interactions in the *reactive*, ternary system nylon-6/caprolactam/water. All of the data sets appear in the Supporting Information.

Maczinger and Tettamanti[30] give four sets of low-pressure, isobaric phase-equilibrium data for the binary water/caprolactam. Tables 15−18 in the Supporting Information show their data.

Giori and Hayes[31] present one set of isothermal phase-equilibrium data for the ternary system water/caprolactam/nylon-6. They carry out nylon-6 polymerizations at 543 K in a laboratory reactor and characterize the resulting phase equilibrium. Table 19 in the Supporting Information shows their experimental data.

3. Methodology

We first characterize the binary interactions between water and caprolactam using the first four data sets[30] (Tables 15−18 in the Supporting Information).

We then simulate the Giori and Hayes experiments[31] to quantify the binary interactions between water/nylon-6 and caprolactam/nylon-6.

3.1. Characterizing the Phase Equilibrium of Water/Caprolactam. Here, we explain how to obtain the binary parameters for water/caprolactam. Our handling of the data consists of testing the data for thermodynamic consistency. We use two consistency tests for our isobaric data sets: a Van Ness et al. test[32] and a Wisniak test.[33] The Wisniak test can be used in a point or area mode; however, we use only the point

test because of the difficulty in accurately of computing integrals of "functions" of our experimental data.

3.1.1. Consistency Test One: Van Ness et al.[32] In this test, we first obtain a redundant data set comprised of temperature, pressure, liquid-mole-fraction, and vapor-mole-fraction measurements ($T-P-x-y$). We then regress only the $T-P-x$ data. After regressing these data, we are able to predict the original pressure data (using $T-x$ data) and vapor-mole-fraction data (using $T-P-x$ data). Consistency test one comes by examining the extent of corroboration between the measured and predicted vapor mole fractions. This test is an indirect application of the Gibbs−Duhem equation because the POLYNRTL model obeys the Gibbs−Duhem equation.

The fundamental phase-equilibrium relation for this analysis is

$$y_i\phi_i P = x_i\gamma_i(x_i,T)\, P_i^{\mathrm{sat}}(T)\exp\left[\frac{v_i}{RT}(P - P_i^{\mathrm{sat}})\right] \quad (12)$$

We compute the activity coefficient γ_i using the POLYNRTL model; it is a function of the liquid composition x_i and temperature T. P_i^{sat} is the vapor pressure, which we compute using an Antoine form:

$$P_i^{\mathrm{sat}} = \exp\left(A_i + \frac{B_i}{T} + C_i \ln T + D_i T_i^{\mathrm{E}}\right) \quad (13)$$

We have neglected vapor-phase nonidealities (fugacity coefficient ϕ_i equals 1) because most of the data are at vacuum conditions; however, one can easily estimate the degree of vapor-phase nonideality occurring at high pressures using the Redlich−Kwong equation of state. Furthermore, the Poynting pressure correction is negligible (the exponential term is 1).

We eliminate the need for vapor-phase composition data by summing eq 12 over all species; for a binary system containing species i and j, we have

$$P = x_i\gamma_i(x_i,T)\, P_i^{\mathrm{sat}}(T) + x_j\gamma_j(x_j,T)\, P_j^{\mathrm{sat}}(T) \quad (14)$$

Using the $T-P-x$ data, we manipulate the six POLYNRTL binary interaction parameters (a_{ij} through c_{ij} for water/caprolactam and caprolactam/water; eq 11) to minimize the following sum-of-squares error (SSE) for each data point k:

$$\mathrm{SSE} = \sum_k \left(\frac{P_k^{\mathrm{obsd}} - P_k^{\mathrm{calcd}}}{P_k^{\mathrm{obsd}}}\right)^2 \quad (15)$$

Once we have the binary interaction parameters, we predict the vapor composition using the original $T-P-x$ data and eq 12. Last, we compute the percent difference in vapor-mole-fraction data vs prediction for each liquid-composition data point:

$$\text{percent deviation} = 100\left(\frac{y^{\mathrm{calcd}} - y^{\mathrm{obsd}}}{y^{\mathrm{obsd}}}\right) \quad (16)$$

We plot the percent deviation vs the liquid mole fraction to characterize the consistency of the observed phase-equilibrium data.

3.1.2. Consistency Test Two: Wisniak.[33] The second consistency test that we use, due to Wisniak, is based on the bubble-point equation for mixtures and utilizes the Clausius−Clapeyron equation. It is fundamentally based and preferable to a combined Redlich−Kister[34]/Herington method[35] for testing the consistency of isobaric phase-equilibrium data.

For each data point i at system temperature T_i, we compute two functions L_i and W_i:

$$L_i = \frac{\sum T_k^0 x_k \Delta s_k^0}{\Delta s} - T_i \quad (17)$$

$$W_i = RT_i\left(\frac{(\sum x_k \ln \gamma_k) - w}{\Delta s}\right) \quad (18)$$

For every species k, at the system pressure, there is a pure-component boiling point T_k^0, a liquid mole fraction x_k, and entropy of vaporization Δs_k^0. In eq 18, Δs is the entropy of mixing of the mixture.

We compute the boiling temperature T_k^0 for each component k by setting the pressure to the system pressure in eq 13 and then backing out the temperature.

We calculate the entropy of vaporization from the enthalpy of vaporization Δh_k^0:

$$\Delta s_k^0 = \frac{\Delta h_k^0}{T_k^0} = \frac{A_k\left(1 - \dfrac{T_k^0}{T_{c,k}}\right)^{B+C(T_k^0/T_{c,k})+D(T_k^0/T_{c,k})^2}}{T_k^0} \quad (19)$$

The critical temperature $T_{c,k}$ as well as the constants A_k through D_k are tabulated in standard reference sources (such as Daubert and Danner[36]) and differ for each chemical species.

We find the activity coefficients from the experimental data using eq 12:

$$\gamma_i = y_i P / x_i P_i^{\mathrm{sat}}(T) \quad (20)$$

We compute the mixture entropy of vaporization for the mixture Δs using the following mixing rule:

$$\Delta s = \sum x_k \Delta s_k^0 \quad (21)$$

Last, we find the w term appearing in eq 18 using

$$w = \sum x_k \ln(y_k/x_k) \quad (22)$$

We perform the point test by computing the ratio of L_i and W_i and plotting this as a function of liquid mole fraction. Inconsistent data contain ratio values that are much different than 1 and do not scatter randomly about 1.

3.1.3. Determining Binary Interaction Parameters from Phase-Equilibrium Data. The Van Ness et al. test[32] effectively regresses binary interaction parameters using $T-P-x$ data only. If the data are judged inconsistent, Prausnitz et al.[37] suggest that we assume that the vapor-phase composition data are incorrect for two reasons:

(i) Accurately measuring y is typically more difficult than measuring x and pressure.

(ii) Composition data at the ends of the composition scale ($y \sim 0$ or 1) are likely to be the least accurate.

If the data are inconsistent and we throw out the vapor-mole-fraction measurements, then we have already obtained binary interaction parameters using the data that we are most confident in ($T-P-x$ data). However, if the data are consistent, then we can use

Table 7. Physical Property Constants for Water and Caprolactam[a]

constant	water	caprolactam
vapor pressure		
A_i	7.3649×10^1	7.4172×10^1
B_i	-7.2582×10^3	-1.0469×10^4
C_i	-7.3037	-6.8944
D_i	4.1653×10^{-6}	1.2113×10^{-18}
E_i	2.0000	6.0000
enthalpy of vaporization	5.2053×10^7	8.3520×10^7
A_i		
B_i	3.1990×10^{-1}	3.7790×10^{-1}
C_i	-2.1200×10^{-1}	0.0000
D_i	2.5795×10^{-1}	0.0000
critical temperature (K)	806.00	647.13

[a] The vapor pressure is computed using eq 13, with units of Pa and temperature units of K. The enthalpy of vaporization is computed using eq 19, with units of J/kmol and temperature units of K.

all of the data to compute activity coefficients by eq 20 and re-regress the binary interaction parameters.

3.2. Characterizing the Ternary, Reactive System Water/Caprolactam/Nylon-6. By completing the first step of this study, section 3.1, we obtain the binary interaction parameters for the system water/caprolactam. We then simulate the Giori and Hayes experiments[31] in order to characterize the binary interactions between water/nylon-6 and caprolactam/nylon-6 segments. We use POLYMERS PLUS to model the batch step-growth polymerizations. However, our methodology is applicable in any polymer process simulator because the kinetics and thermodynamics models are reproduced from open literature sources.

We simulate a 0.000 077 m^3 (77 mL) reactor using the Arai et al. kinetic scheme[18] and the binary interaction parameters for water/caprolactam. We maintain a vapor−liquid system throughout the polymerization. After reaction equilibrium is reached in the closed vessel, we predict the final liquid and vapor compositions, as well as the final pressure. We give our simulation procedure below, with specifications given in Giori and Hayes.[31]

1. Charge the batch reactor of a specified size with a specified amount of water and caprolactam.

2. Set the reactor to a specified temperature and enforce VLE using the POLYNRTL activity-coefficient model, thereby predicting the liquid−vapor composition and reactor pressure.

3. Allow the nylon-6 polymerization reaction to proceed until reaction equilibrium is established.

4. Report the final liquid and vapor compositions, as well as the final reactor pressure.

Because we only have five sets of batch reaction data from Giori and Hayes,[31] we must minimize the number of free parameters in fitting the reaction data. We regress the b_{ij} parameters for water/nylon-6 and caprolactam/nylon-6 segment interactions. We fix the a_{ij} and c_{ij} parameters to zero.

We vary these four binary interaction parameters, two for each binary interaction, until we match the outlet compositions and pressures from the data of Giori and Hayes.[31] The resulting binary interaction parameters characterize the systems, water/nylon-6 and caprolactam/nylon-6 segments.

4. Results and Discussion

4.1. Binary Interaction Parameters for Water/Caprolactam. Table 7 contains the pertinent physical property constants for water and caprolactam, found in Daubert and Danner.[36] We need these parameters to compute the vapor pressure and enthalpy of vaporization.

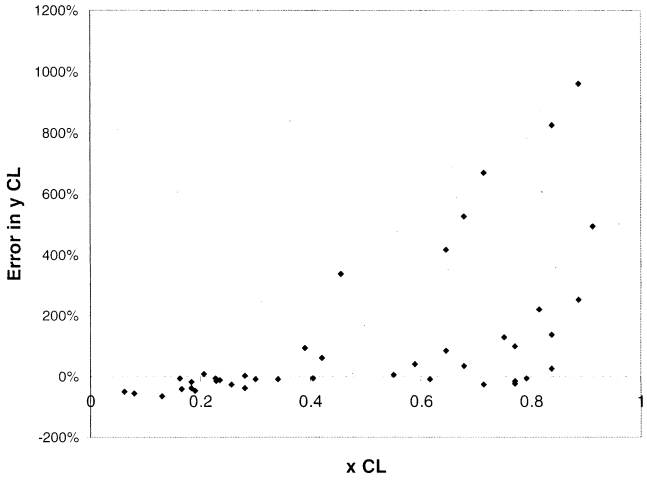

Figure 3. Percent error in vapor-mole-fraction prediction vs liquid mole fraction for caprolactam for all water/caprolactam data sets (Van Ness et al. test[32]).

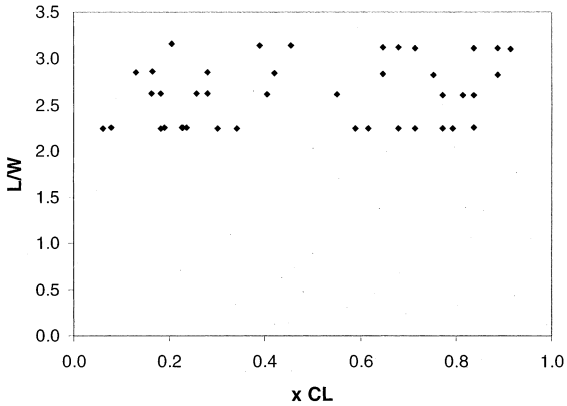

Figure 4. L/W ratio vs caprolactam liquid mole fraction for all water/caprolactam data sets (Wisniak test[33]).

Figure 3 shows the results of the Van Ness et al. test[32] for thermodynamic consistency: a plot of the percent error in vapor mole fraction vs liquid mole fraction for caprolactam.

Consistent data show small, randomly distributed errors around the x axis. Inconsistent data give large, nonrandomly distributed errors. It is clear from Figure 3 that all data sets are inconsistent.

Similarly, for the Wisniak test,[33] we show a ratio plot in Figure 4.

Consistent data would reveal a ratio that is more-or-less 1 for each liquid-mole-fraction data point. However, all of the data show a bias, with the ratio being 2 or higher for all sets. This again suggests the presence of a systematic error in the phase-equilibrium data.

Unfortunately, consistent tests never tell us *which* data are not constant. As stated previously, we assume that the vapor-phase composition data are incorrect;[37] unfortunately, no error analysis was performed in the works of Maczinger and Tettamanti[30] and Giori and Hayes.[31]

Table 8 summarizes the regressed binary interaction parameters using only $T-P-x$ data.

Figure 5 shows the plot of the POLYNRTL parameters τ_{ij} vs temperature.

Table 8. Regression Results for POLYNRTL Binary Interaction Parameters for Water/Caprolactam (Based on $T-P-x$ Data Only)

POLYNRTL binary interaction parameter	value (temperature units are K)
$a_{water/CL}$	−0.313
$a_{CL/water}$	0.628
$b_{water/CL}$	−15.4
$b_{CL/water}$	−13.7
$c_{water/CL}$	0.0495
$c_{CL/water}$	−0.0898

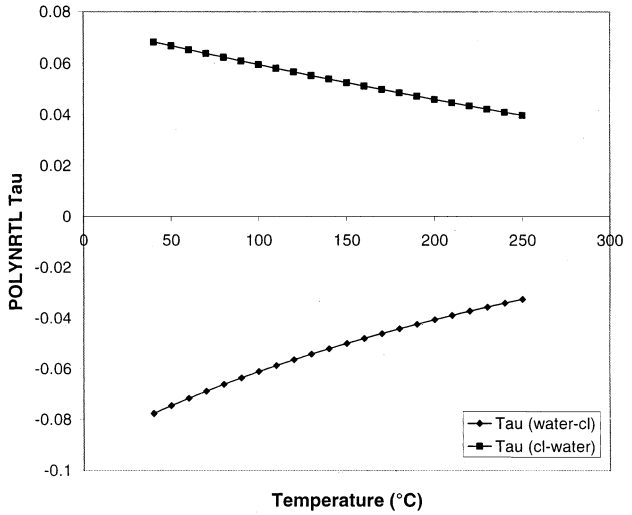

Figure 5. Predicted value of the POLYNRTL binary parameter τ_{ij} for water/caprolactam and caprolactam/water.

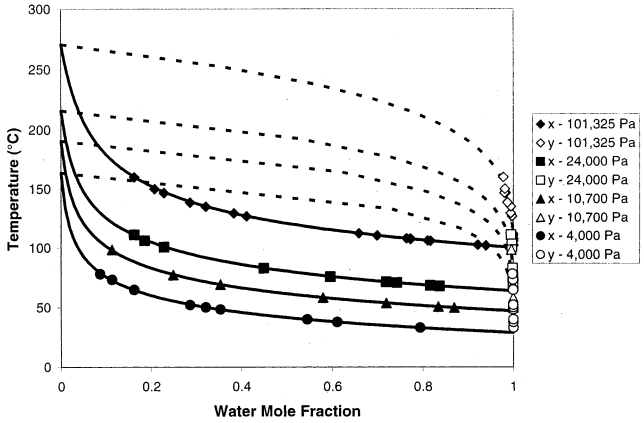

Figure 6. Water/caprolactam $T-x-y$ diagram. The solid lines represent the POLYNRTL activity coefficient model predictions for the liquid mole fraction, while the dotted lines represent the POLYNRTL activity coefficient model predictions for the vapor mole fraction.

The binary interaction parameter τ_{ij} is not significantly different from zero over a wide temperature range. This suggests that the energy of interaction does not largely differ between unlike interactions and like interactions (i.e., near-ideal solution behavior).

We plot the experimental data vs POLYNRTL model calculations for each of the four isobars in Figure 6.

The POLYNRTL model accurately correlates the phase-equilibrium data. Furthermore, assuming ideal behavior in the vapor and liquid phases gives nearly identical predictions. *Therefore, we may safely neglect nonidealities in water/caprolactam solutions under vacuum.* This means that we can set the fugacity and activity coefficients to 1 when simulating water/caprolactam mixtures under vacuum conditions. However, as we shall see below, the ternary system water/caprolactam/nylon-6 shows moderate deviations from ideal behavior.

Table 9. Comparison of Model Predictions with Giori and Hayes Polymerization Data[31]

caprolactam liquid mole fraction	water liquid mole fraction	water vapor mole fraction	total pressure (Pa)
	Data		
0.096	0.012	0.74	571 000
0.097	0.0249	0.85	974 000
0.099	0.0387	0.886	1 400 000
0.101	0.0515	0.89	1 830 000
0.106	0.065	0.91	2 160 000
	Model Prediction		
0.087	0.012	0.69	537 000
0.086	0.025	0.84	1 010 000
0.086	0.039	0.90	1 440 000
0.085	0.052	0.93	1 830 000
0.085	0.066	0.95	2 180 000
	% Error		
−9.38	0.00	−6.76	−6.02
−11.34	0.40	−1.18	4.02
−13.13	0.78	1.58	3.25
−15.84	0.97	4.49	0.28
−19.81	1.54	4.40	0.99

4.2. Binary Interaction Parameters for Water/Nylon-6 and Caprolactam/Nylon-6 Segments. With these binary interaction parameters, we turn to simulating the Giori and Hayes data.[31] We manipulate the second binary interaction parameters b_{ij} for small molecule/nylon-6 segment interactions. We obtain model predictions and compare them with the Giori and Hayes data in Table 9.

The binary interaction parameters are $b_{water/nylon-6\ segment} = 297$, $b_{nylon-6\ segment/water} = -601$, $b_{caprolactam/nylon-6\ segment} = 265$, and $b_{nylon-6\ segment/caprolactam} = 207$ (temperature units in K).

The average model prediction error for water composition is 0.74%. Note that we are most interested in this composition because it significantly impacts the final polymer properties, such as polymer molecular weight and conversion. The model underpredicts the final caprolactam liquid composition by about 13.9%. The average error for the final pressure prediction is −0.51%.

Table 10 compares the Giori and Hayes data[31] with the three previous literature models, along with ideal vapor−liquid predictions (fugacity−activity coefficients equal 1).

The Jacobs−Schweigman model[20] is ill-applied; system pressures for the Giori and Hayes data[31] range from 5 to 21 atm. The predictions for this model are about an order of magnitude different from the experimental data. This unacceptable level of error illustrates the inappropriateness of the Jacobs−Schweigman model for modeling general phase equilibrium.

The Fukumoto model predictions[21] are the best out of the three literature models: the average error is −31%. The Tai et al. model[12] is surprisingly inaccurate, given that it is the most advanced out of the three. The average error of the Tai et al. model is 317%. Lastly neglecting nonideality results in water liquid composition errors of 7.52%. Because water-concentration terms in the kinetic expressions are proportional to water mole fractions in the liquid phase, we can expect that this error would cause errors of ca. 8% when computing reaction-rate terms. A likely explanation as to why ideal behavior approximates the Giori and Hayes data[31] is that the excess Gibbs energy of mixing is low when the

Table 10. Predictions for Liquid-Phase Water Mole Fractions of Previous Literature Models and the Ideal Model and Comparison with Experimental Data of Giori and Hayes[31]

liquid-phase water mole-fraction data	Jacobs−Schweigman[20]	Fukumoto[21]	Tai et al.[12]	ideal (fugacity and activity coefficients set to 1)
0.0119	0.0014	0.0101	0.0607	0.0129
0.0249	0.0014	0.0181	0.1100	0.0269
0.0387	0.0014	0.0248	0.1509	0.0411
0.0515	0.0014	0.0323	0.1974	0.0554
0.0650	0.0014	0.0382	0.2338	0.0698

liquid-phase water mole-fraction data	Jacobs−Schweigman error (%)	Fukumoto error (%)	Tai et al. error (%)	ideal error (%)
0.0119	−88	−15	410	8.47
0.0249	−94	−27	342	7.92
0.0387	−96	−36	290	6.21
0.0515	−97	−37	283	7.64
0.0650	−98	−41	260	7.33

composition is at extreme values (the polymer fraction is near 0 or 1).

By way of comparison, our new phase-equilibrium model generates an average prediction error for the water liquid mole fraction of 1%. More importantly, it allows us to make phase-equilibrium predictions in any binary or ternary mixture that primarily contains water, caprolactam, and nylon-6 at any specified temperature and pressure.

We note that we do not have enough batch reaction data to determine a unique set of binary interaction parameters for water/nylon-6 and caprolactam/nylon-6 segments. Therefore, we have regressed the minimum number of binary interaction parameters possible, setting a_{ij} and c_{ij} to zero and only regressing b_{ij}. The fit to the available data is good; however, because of the limited data, we caution against extrapolation far away from 270 °C and outside of the pressure range of 570−2200 kPa.

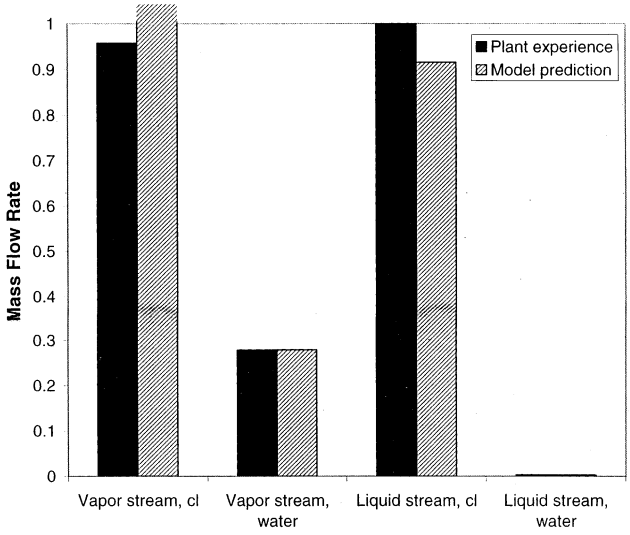

Figure 7. Mass flow rates exiting the condenser: model prediction vs plant experience (all values have been normalized using the largest flow rate).

5. Validation of Regressed Binary Interaction Parameters

We consider two model predictions to be good indicators of the quality of our binary interaction parameters: condenser performance and devolatilization in finishing reactors. Here, we perform exploratory simulations of a commercial condenser and two wiped-film evaporators.

We start with the analysis of the condenser. The feed contains a mixture of caprolactam and water. The condenser operates at a temperature of 483 K and a pressure of 53 kPa. When we simulate the condenser as a single flash unit, we get predictions for the liquid and vapor stream flow rates. Figure 7 compares our predictions with plant experience.

The vapor-phase flow rates of caprolactam and water are predicted with an average error of about 4%. The model underpredicts the liquid-phase component flow rates of caprolactam and water by about 9%.

It is significant to note the split fractions: the data show that about 49% of the caprolactam is vaporized, while 99% of the water is vaporized. Our phase-equilibrium predictions nearly match the data, showing 53% for caprolactam vaporization and 99% for water vaporization.

In our model of the first wiped-film evaporator, we simulate a vapor−liquid plug-flow reactor, with a feed stream containing 2.00×10^{-3} parts by weight water, 1.54×10^{-1} parts caprolactam, and 8.44×10^{-1} parts semiterminated nylon-6. The molecular weight of the incoming polymer is 11.5 kg/mol. The reactor is operating at ca. 520 K and 4 kPa with a residence time of 600 s.[10]

By way of validation, we are looking at the devolatilization behavior of small molecules, namely, caprolactam. From prior experience,[38] we know that devolatilization of caprolactam is mass-transfer-limited. Therefore, if we ignore mass-transfer limitations in the model, we should devolatilize too much caprolactam and therefore underpredict the mass fraction of caprolactam in the exiting melt stream.

Our model predicts a caprolactam mass fraction in the exit stream of 1.1%, while plant data show 2.9% for similar operating conditions. This is an underprediction by 62%. This shows that our phase-equilibrium predictions are in the right direction considering mass-transfer limitations. What would not be reasonable is an equilibrium prediction for the caprolactam percentage that is actually more than the mass-transfer-limited case. Regarding the caprolactam mass percentage in the exiting melt, the equilibrium case should always be lower than the mass-transfer-limited case.

Now we simulate a second wiped-film evaporator. Once again, we consider a vapor−liquid plug-flow reactor, with a feed stream containing 2.41×10^{-3} parts by weight water, 1.4×10^{-1} parts caprolactam, and 8.58

$\times 10^{-1}$ parts semiterminated nylon-6. The molecular weight of the incoming polymer is 9.8 kg/mol. This reactor is operating at ca. 523 K and 4.67 kPa with a residence time of 1740 s.[10]

Our model predicts a caprolactam mass fraction in the exit stream of 1.5%, while plant data show 2.7% for similar operating conditions. This is an underprediction by 44%. This again shows that our phase-equilibrium calculations are in the right direction considering mass-transfer limitations.

Regarding the wiped-wall evaporator studies, one may ask the following valid question: may we approximate the error of the phase-equilibrium model from these results, as in the condenser study? Unfortunately, this is not possible because we do not know to what extent mass-transfer limitations are affecting the reactor performance. In other words, if there is no mass-transfer limitation, the phase-equilibrium model is in error by −62 to −44%. If there is a strong mass-transfer limitation, then the phase-equilibrium model may have little or no error.

6. Simulating Integrated Industrial Nyon-6 Production Trains

Previous attempts at nylon-6 *integrated process modeling* were hindered by the lack of a fundamental thermodynamic phase-equilibrium model. For example, Nagasubramanian and Reimschuessel[39] simulated the molecular weight buildup in the finishing stage by first "instantaneously" removing all water from the polymerization mass while ignoring caprolactam devolatilization. There is no corresponding unit operation that can perform this separation in an actual plant. Furthermore, this assumption has led Tirrell et al.[40] to an unusual conclusion: that it is preferable to perform molecular weight buildup and monomer conversion in a single reactor. To have adequate molecular weight buildup, we need to enforce low water concentrations. However, to do this, we typically use severe operating conditions, such as high vacuum in melt processes,[10] to remove most of the water. In doing so, we cannot avoid losing a significant amount of the caprolactam to the vapor phase. Therefore, equilibrium thermodynamics clearly suggests that it is impractical to try to obtain both molecular weight buildup and monomer conversion in the same reactor.

Assuming an instantaneous and complete water removal was necessary in the past because researchers did not have access to a fundamental thermodynamic model. However, with our new phase-equilibrium model, we are able to simulate *any* unit operation that involves caprolactam, water, and nylon-6 at multiphase conditions. These include flash units and condensers. Therefore, we simulate multiphase reactors with condensers that return unreacted monomer back to the inlet of the train. In particular, we simulate two commercial technologies: a melt train and a bubble-gas kettle train. All details such as the unit operation configuration, feed conditions, and operating conditions are available in the patent literature.

This section is not concerned with developing a *validated* simulation model for these processes; this endeavor is well beyond the scope of this paper. Therefore, we do not make detailed comparisons between model predictions and plant data. We wish only to illustrate the utility of our phase-equilibrium model in simulating entire manufacturing trains.

6.1. Melt Train.

We simulate a typical commercial melt train involving four reactors.[10] The first two reactors carry out monomer conversion; the third and fourth reactors carry out devolatilization and molecular weight buildup. Figure 8 shows the process-flow diagram for this train.

The makeup stream contains 5.35×10^{-5} kg/s of water, 0.0120 kg/s of caprolactam, and 2.01×10^{-5} kg/s of AA terminator. We have assumed a production rate of about 0.0112 kg/s of polymer or 89 pounds per hour (pph) and have calculated approximate flow rates for water and terminator based on refs 10 and 41−44.

The first vessel is a continuous stirred-tank reactor (CSTR), STAGE-1 in Figure 8. The residence time is 8100 s, the temperature is 488 K, and the pressure is 545 kPa.

The second vessel is a plug-flow reactor (PFR), STAGE-2 in Figure 8. The feed to this vessel enters a vapor headspace, which we simulate using a flash unit at reactor conditions (HD-SPACE in Figure 8). Vapor from this flash enters the reflux condenser (RFLX-CND in Figure 8). Most of the caprolactam is returned back to the reactor headspace, while a mixture of caprolactam and water goes to the train condenser (CONDENSE in Figure 8). The reactor has a residence time of 28 800 s, a temperature of 498 K, and a pressure of 66.7 kPa.

The third reactor is a vapor−liquid plug-flow reactor, EVAPORAT in Figure 8. The vapor phase is removed via a vacuum system (EVAP-FL in Figure 8) and enters the train condenser CONDENSE. This reactor has a residence time of 1200 s, a temperature of 523 K, and a pressure of 2.33 kPa.

The fourth reactor is a vapor−liquid plug-flow reactor, FINISHER in Figure 8. The vapor phase is removed via a vacuum system (FIN-FL in Figure 8) and also enters the train condenser CONDENSE. We used a sweep-steam mass flow rate of ca. one-quarter of that of the polymer flow rate entering the reactor. This reactor has a residence time of 7200 s, a temperature of 536 K, and a pressure of 4 kPa.

The train condenser CONDENSE recovers the unreacted monomer and sends it back to the inlet of the train. Uncondensed species, mostly water, leave in a waste stream. The condenser operates at an assumed pressure of 101.325 kPa and an assumed temperature of 403 K.

Table 11 summarizes the vessel operating conditions.

We model mass-transfer limitations in the evaporator and finisher reactors using two-film diffusion theory.[45] The diffusion coefficient is relatively high for water in nylon-6 melts,[38] and we assume that the evaporator and finisher reactors generate a large interfacial surface area. Therefore, we set the water mass-transfer coefficient to 1×10^{-2} m/s and set the mass-transfer coefficient for caprolactam to 5×10^{-4} m/s.

Table 12 shows the predicted mass flow rates for water, caprolactam, cyclic dimer, and nylon-6 exiting each reactor. Furthermore, the table reports number-average molecular weight predictions (M_n).

We see that all of the monomer conversion (about 81% in this case) takes place in the first two reactors. However, because of elevated moisture levels, the molecular weight only grows to about 10.7 kg/mol. In the third and fourth reactors, we remove nearly all of the water and double the polymer molecular weight. Our final molten polymer product has a flow rate of 1.16×10^{-2} kg/s, the polymer has a number-average molecular

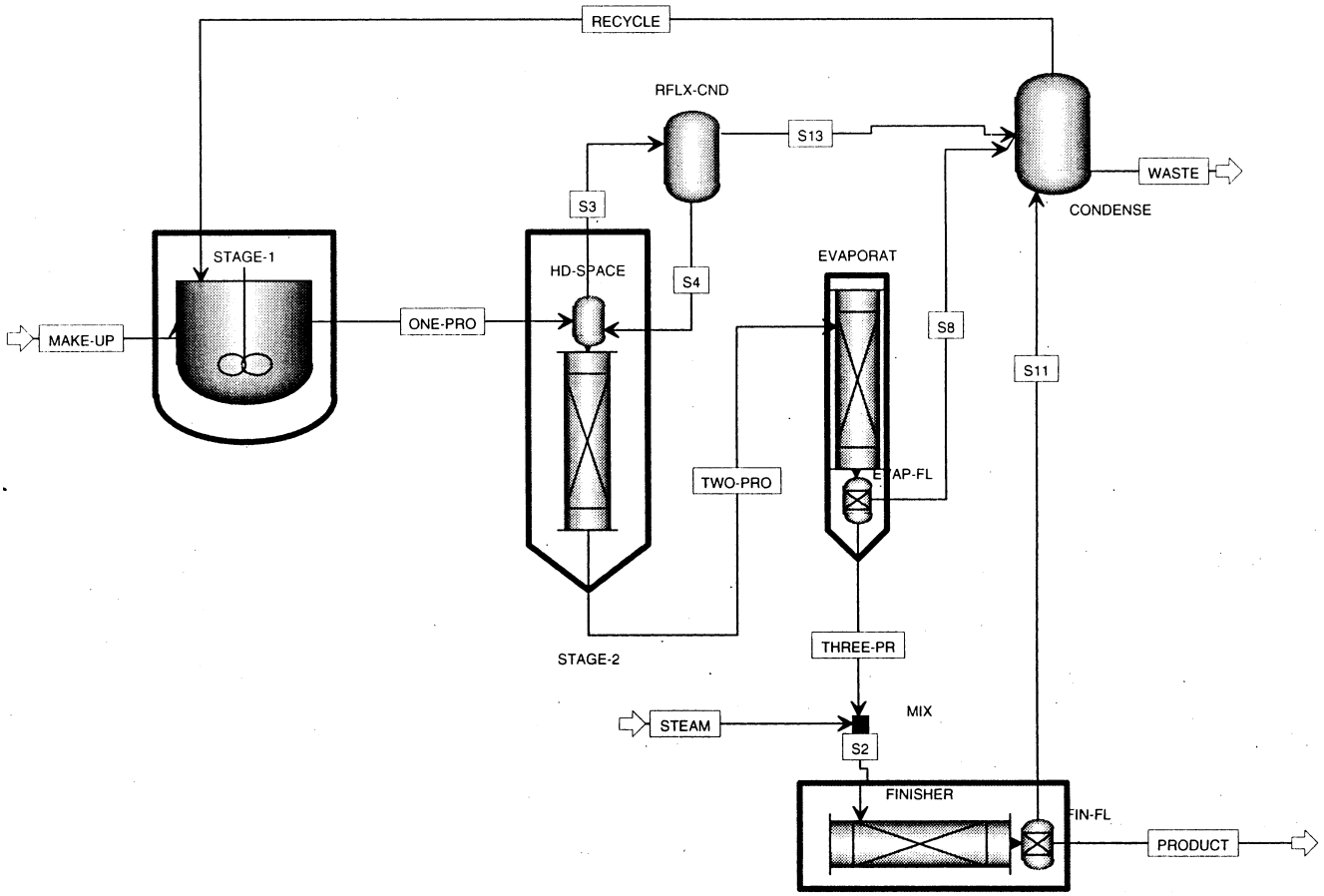

Figure 8. Four-reactor nylon-6 manufacturing process. Most of the monomer conversion takes place in the first two reactors, while the molecular weight buildup occurs in the third and fourth reactors. The second vessel has a reflux condenser, while the entire train has a condenser to recycle the unreacted monomer.

Table 11. Operating Conditions for Each Reactor in the Four-Reactor Train Depicted in Figure 8

unit operation	temp (K)	pressure (kPa)	residence time (s)
first reactor	488	545	8100
second reactor	498	66.7	28800
reflux condenser	403	66.7	
third reactor	523	2.33	1200
fourth reactor	536	4.00	7200
train condenser	403	101.325	

Table 12. Model Predictions for Liquid-Phase Mass Flow Rates Exiting Each Reactor (Process Flow Diagram in Figure 8)

reactor	caprolactam (kg/s)	water (kg/s)	cyclic dimer (kg/s)	nylon-6 (kg/s)	M_n (kg/mol)
1	2.85×10^{-4}	9.36×10^{-3}	7.39×10^{-6}	5.34×10^{-3}	2.9
2	5.71×10^{-5}	2.81×10^{-3}	2.73×10^{-5}	1.19×10^{-2}	10.7
3	3.10×10^{-7}	1.69×10^{-3}	2.87×10^{-5}	1.20×10^{-2}	11.7
4	1.25×10^{-6}	1.92×10^{-4}	4.21×10^{-5}	1.16×10^{-2}	18.3

weight of 18.3 kg/mol, and the caprolactam content is about 1.6%.

The molecular weight prediction is close to plant experience of melt trains, about 18 kg/mol. The caprolactam content is also close: plant experience ranges from 0.7 to 1.5%.

Additional predictions now follow: 2.44×10^{-4} kg/s, or 85%, of the incoming water is lost to the vapor phase in the second reactor, while virtually all of the water is vaporized in the third reactor. Almost no caprolactam is lost in the second reactor because of the presence of the reflux condenser; however, about 2.83×10^{-3} kg/s of monomer is devolatilized in the third and fourth reactors (36% of incoming caprolactam). Previous analyses, such as those by Nagasubramanian and Reimschuessel[39] and by Tirrell et al.,[40] would assume that no water is lost in the first two vessels (approximated roughly by one vessel in their studies) and no caprolactam is lost in the third and fourth vessels (approximated roughly by one vessel in their studies). Our simulation, which contains phase-equilibrium and mass-transfer models, shows that these are poor assumptions for a typical commercial melt train.

6.2. Bubble-Gas Kettle Train. We now simulate a typical commercial bubble-gas kettle train.[13] This train has three agitated kettles as in Figure 9.

A total of 2.08×10^{-3} kg/s of caprolactam enters the first vessel, along with 7.73×10^{-4} kg/s of steam.

We model the first kettle, KETTLE1 in Figure 9, as a vapor−liquid CSTR with exit liquid and vapor streams. Steam and lactam are fed to this reactor. This kettle operates at 527 K and 579 kPa. This kettle has a residence time of 9300 s.

We assume that the second kettle, KETTLE2 in Figure 9, is mass-transfer-limited. We again model it as a multiphase CSTR utilizing two-film theory to compute the evaporation rate of volatiles. A total of 4.91×10^{-5} kg/s of inert gas (assumed to be nitrogen) is bubbled through the reaction mixture to remove volatiles. We assume that the mass-transfer coefficients are 1 and 1×10^{-4} m/s for water and caprolactam, respectively. This kettle has a residence time of 13 400 s, a temperature of 528 K, and a pressure of 101.325 kPa.

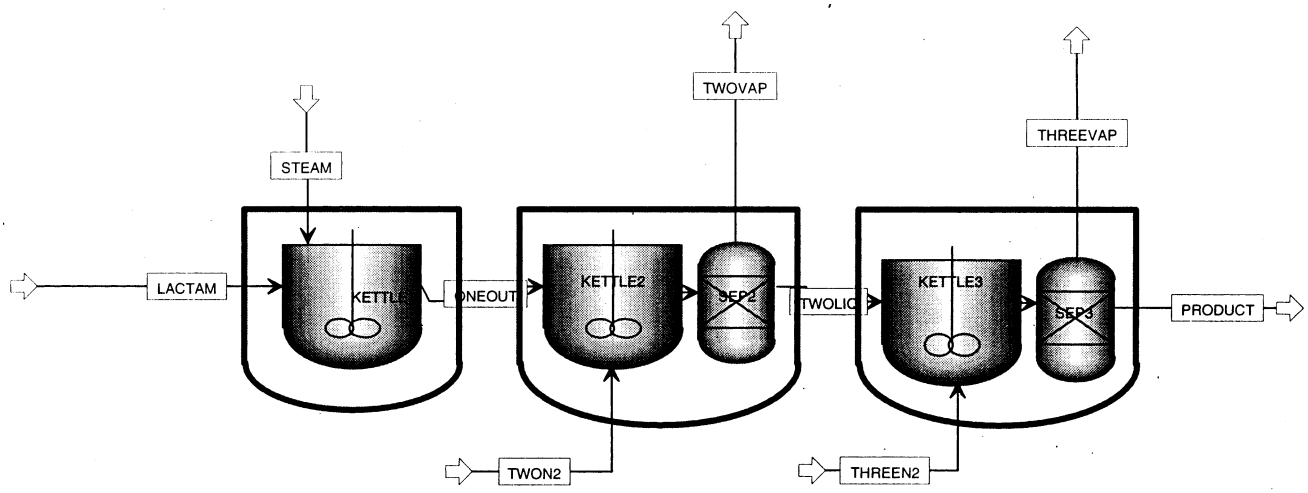

Figure 9. Three-reactor nylon-6 manufacturing process. Lactam and water are fed to the first multiphase kettle, while inert gas flow devolatilizes the second and third vessels.

Table 13. Operating Conditions for Each Kettle Depicted in Figure 9

kettle	temp (K)	pressure (kPa)	residence time (s)	steam/nitrogen flow rate (kg/s)
1	527	579.	9300	7.73×10^{-4} (steam)
2	528	101.325	13400	4.91×10^{-5} (nitrogen)
3	528	101.325	13400	4.91×10^{-5} (nitrogen)

Table 14. Predicted Liquid-Stream Compositions Exiting Each Kettle (Process Flow Diagram Depicted in Figure 9)

reactor	caprolactam (kg/s)	water (kg/s)	cyclic dimer (kg/s)	nylon-6 (kg/s)	M_n (kg/mol)
1	4.83×10^{-4}	4.77×10^{-5}	6.45×10^{-6}	1.51×10^{-3}	5.2
2	2.37×10^{-4}	3.99×10^{-6}	8.71×10^{-6}	1.67×10^{-3}	12.4
3	1.89×10^{-4}	1.34×10^{-6}	9.56×10^{-6}	1.69×10^{-3}	20.6

The third kettle, KETTLE3 in Figure 9, is identical to the second kettle regarding operating conditions.

Table 13 summarizes the vessel operating conditions.

Table 14 shows the liquid-phase flow rates, compositions, and polymer molecular weights coming out of each kettle.

With this train, we produce 1.69×10^{-3} kg/s of nylon (81% conversion), with 10% caprolactam coming out of the third kettle. The molecular weight of the polymer is 20.6 kg/mol. Both the caprolactam content and molecular weight predictions are close to plant experience of bubble-gas kettle trains: about 9% and 21 kg/mol for caprolactam and molecular weight, respectively.

In the first kettle, 75% of the incoming water exits in the vapor stream, along with 4% of the incoming caprolactam. In the second kettle, the corresponding percentages are 98% and 18%, respectively. Lastly, the third kettle devolatilizes 80% of the incoming water and 34% of the incoming caprolactam.

This example again shows that an incomplete devolatilization based on a more detailed analysis of the phase equilibrium is more realistic. Using the previous assumptions regarding nylon phase behavior would have resulted in severe prediction inaccuracies.

6.3. Example Summary. These two applications illustrate that we are no longer bound by unrealistic assumptions, such as no or instantaneous water removal, while ignoring caprolactam devolatilization. In fact, we obtain a high level of detail in our simulations, including an analysis of the monomer-recovery portion that exists for every realistic manufacturing process. This high level of modeling detail is possible using our fundamental phase-equilibrium model for water/caprolactam/nylon-6.

7. Conclusions

We have advanced nylon-6 process-simulation technology by developing and documenting a fundamental phase-equilibrium model. It represents a step forward toward the generation of a single, consistent model that describes the phase behavior of all commercially significant nylon polymerization−depolymerization technologies.

In creating this model, we use phase-equilibrium data to characterize the ternary system, water/caprolactam/nylon-6. We illustrate adequate treatment for inconsistent thermodynamic data, including the generation of a coherent set of POLYNRTL binary interaction parameters. We then show how to simulate the reactive system, water/caprolactam/nylon-6, to extract binary interaction parameters for water/nylon-6 and caprolactam/nylon-6 segments. Our model predicts the liquid mole fraction of water with an average error of 1%; previous literature models sometimes generate predictions that are more than an order of magnitude in error.

After generating a complete model for the phase equilibrium for water/caprolactam/nylon-6, we validate the interaction parameters by performing exploratory simulations of commercial manufacturing processes. We simulate a condenser and match the split fraction for water (99%). We predict a caprolactam split fraction of 53%, which approximates the real split fraction of 49%.

We also simulate two commercial wiped-film evaporators and show that the models underpredict the mass fraction of caprolactam in the exit polymer stream. This is in accordance with expectations: we did not simulate mass-transfer limitations and, therefore, the amount of caprolactam predicted to be in the liquid phase should be low when compared with plant data.

Last, we demonstrate two applications of our new phase-equilibrium model that simulate two integrated nylon-6 production processes: a melt train and a bubble-gas kettle train. We simulate wide ranges of temperature and pressure conditions, with temperature ranging from 403 to 536 K and pressure ranging from 2.33 to 545 kPa. We perform fundamental kinetic, thermodynamic, and mass-transfer calculations to make detailed

predictions about reactor products. These predictions could not be made in the past without a fundamental phase-equilibrium model.

Acknowledgment

We thank Alliant Techsystems, Aspen Technology (particularly, Jila Mahalec, past Director of Worldwide University Programs; Dustin MacNeil, current Director of Worldwide University Programs; Joseph Boston, Senior Corporate Advisor and Past President; and Larry Evans, Board Chairman), China Petroleum and Chemical Corp. (SINOPEC), China National Petroleum Corp., Honeywell Specialty Materials, and Honeywell International Foundation for supporting the computer-aided design educational programs at Virginia Tech. We also thank Paul Mathias, David Tremblay, and Yuhua Song, Polymer Industry Business Unit, Aspen Technology, for their helpful input to this study.

Supporting Information Available: Tables of phase-equilibrium data of the system water/caprolactam at various pressures and of the system water/caprolactam/nylon-6. This material is available free of charge via the Internet at http://pubs.acs.org.

Nomenclature

a_{ij} = binary interaction parameter coefficient for the binary $i-j$
A_i^0 = preexponential factor for uncatalyzed forward reaction i, kg/mol·s
A_i^c = preexponential factor for catalyzed forward reaction i, kg/mol·s
b_{ij} = binary interaction parameter coefficient for the binary $i-j$, K
c_{ij} = binary interaction parameter coefficient for the binary $i-j$
E_i^0 = activation energy for uncatalyzed forward reaction i, J/mol
E_i^c = activation energy for catalyzed forward reaction i, J/mol
ΔH_i = enthalpy of reaction i, J/mol
K_i' = equilibrium constant for reaction i
k_i = forward rate constant for reaction i, kg/mol·s
k_i' = reverse rate constant for reaction i, kg/mol·s
L = Wisniak consistency test function, K
n = degree of polymerization
P = pressure, Pa
P_i = partial pressure of species i, Pa
P_i^{vap} = vapor pressure for species i, Pa
R = ideal gas law constant, J/mol·K
ΔS_i = entropy of reaction i, J/mol·K
T = temperature, K
T_i^0 = boiling point for component i, K
w = Wisniak consistency test function
W = Wisniak consistency test function, K
x_i = liquid-phase mole fraction of species i
y_i = vapor-phase mole fraction of species i
α_{ij} = POLYNRTL nonrandomness factor for the binary $i-j$
γ_i = activity coefficient for species i
Δh_i^0 = enthalpy of vaporization at the boiling point for component i, J/mol
Δs = mixture entropy of vaporization, J/mol·K
Δs_i^0 = entropy of vaporization at the boiling point for component i, J/mol·K
τ_{ij} = POLYNRTL binary interaction parameter for the binary $i-j$

Literature Cited

(1) Kohan, M. I., Ed. *Nylon Plastics*; Wiley: New York, 1973.

(2) Hajduk, F. Nylon Fibers. *Chemical Economics Handbook*; SRI International: Menlo Park, CA, Mar 1−2, 2002.

(3) Davenport, R. E.; Riepl, J.; Sasano, T. Nylon Resins. *Chemical Economics Handbook*; SRI International: Menlo Park, CA, Jul 1−4, 2001.

(4) Giori, C.; Hayes, B. T. Hydrolytic Polymerization of Caprolactam. I. Hydrolysis−Polycondensation Kinetics. *J. Polym. Sci., Polym. Chem. Ed.* **1970**, *8*, 335−349.

(5) Agrawal, A. K.; Devika, K.; Manabe, T. Simulation of Hydrolytic Polymerization of Nylon-6 in Industrial Reactors: Part I. Mono-Acid-Stabilized Systems in VK Tube Reactors. *Ind. Eng. Chem. Res.* **2001**, *40*, 2563−2572.

(6) Gupta, S. K.; Kunzru, D.; Kumar, A.; Agarwal, K. K. Simulation of Nylon-6 Polymerization in Tubular Reactors with Recycle. *J. Appl. Polym. Sci.* **1983**, *28*, 1625−1640.

(7) Amon, M.; Denson, C. D. Simplified Analysis of the Performance of Wiped-Film Polycondensation Reactors. *Ind. Eng. Fundam.* **1980**, *19*, 415−420.

(8) Gupta, A.; Gupta, S. K.; Ghandi, K. S.; Mehta, M. H.; Padh, M. R.; Soni, A. V.; Ankleswaria, B. V. Modeling of Hydrolytic Polymerization in a Semi-Batch Nylon-6 Reactor. *Chem. Eng. Commun.* **1992**, *113*, 63−89.

(9) Twilley, I. C.; Roth, D. W. H.; Lofquist, R. A. Process for the Production of Nylon-6. U.S. Patent 3,558,567, 1971.

(10) Yates, S. L.; Cole, C. J.; Wiesner, A. H.; Wagner, J. W. Two-Stage Hydrolysis Process for the Preparation of Nylon-6. U.S. Patent 4,310,659, 1982.

(11) http://www.oit.doe.gov/chemicals/pdfs/nylon.pdf (accessed Sept 2002).

(12) Tai, K.; Arai, Y.; Tagawa, T. The Simulation of Hydrolytic Polymerization of ϵ-Caprolactam in Various Reactors. *J. Appl. Polym. Sci.* **1982**, *27*, 731−736.

(13) Russell, W. N.; Wiesner, A. H.; Snider, O. E. Continuous Polymerization of ϵ-Caprolactam. U.S. Patent 3,294,756, 1966.

(14) Gaymans, R. J.; Amirtharaj, J.; Kamp, H. Nylon-6 Polymerization in the Solid State. *J. Appl. Polym. Sci.* **1982**, *27*, 2513−2526.

(15) Sifniades, S. Recovery of Caprolactam from Waste Carpets. European Patent Application 0676395A1, 1995.

(16) Bokis, C. P.; Orbey, H.; Chen, C. C. Properly Model Polymer Processes. *Chem. Eng. Prog.* **1999**, *95* (4), 39−52.

(17) Loth, W.; Vonend, J.; Lehnen, U.; Kory, G.; Hungenberg, K. D. Simulation of the Entire Process for the Development and Optimization of Polymer Process Concepts. *DECHEMA Monogr.* **1998**, *134*, 545−556.

(18) Arai, Y.; Tai, K.; Teranishi, H.; Tagawa, T. Kinetics of Hydrolytic Polymerization of ϵ-Caprolactam: 3. Formation of Cyclic Dimer. *Polymer* **1981**, *22*, 273−277.

(19) Barrera, M.; Ko, G.; Osias, M.; Ramanathan, M.; Tremblay, D. A.; Chen, C. C. Polymer Component Characterization Method and Process Simulation Apparatus. U.S. Patent 5,687,090, 1997.

(20) Jacobs, H.; Schweigman, C. Mathematical Model for the Polymerization of Caprolactam to Nylon-6. *Proc. Fifth Eur./Second Int. Symp. Chem. React. Eng.* **1972**, *B7*, 1−26.

(21) Fukumoto, O. Equilibria Between Polycapramide and Water. I. *J. Polym. Sci.* **1956**, *XXII*, 263−270.

(22) Chen, C. C. A Segment-based Local Composition Model for the Gibbs Energy of Polymer Solutions. *Fluid Phase Equilib.* **1993**, *83*, 301−312.

(23) Flory, P. J. Thermodynamics of High Polymer Solutions. *J. Chem. Phys.* **1942**, *10*, 51−61.

(24) Huggins, M. L. Some Properties of Solutions of Long-Chain Compounds. *J. Phys. Chem.* **1942**, *46*, 151−158.

(25) Fredenslund, A.; Jones, R. L.; Prausnitz, J. M. Group Contribution Estimation of Activity Coefficients in Nonideal Liquid Mixtures. *AIChE J.* **1975**, *21*, 1086−1099.

(26) Redlich, O.; Kwong, J. N. S. On the Thermodynamics of Solutions. V. An Equation of State. Fugacities of Gaseous Solutions. *Chem. Rev.* **1949**, *44*, 233−244.

(27) Van Krevelen, D. W. *Properties of Polymers*; Elsevier: New York, 1990.

(28) Renon, H.; Prausnitz, J. M. Local Compositions in Thermodynamic Excess Functions for Liquid Mixtures. *AIChE J.* **1968**, *14*, 135−144.

(29) Prausnitz, J. M.; Lichtenthaler, R. N.; de Azevedo, E. G. *Molecular Thermodynamics of Fluid-Phase Equilibrium*, 3rd ed.; Prentice Hall: Englewood Cliffs, NJ, 1999; p 261.

(30) Maczinger, J.; Tettamanti, K. Phase Equilibrium of the System Caprolactam/Water. *Period. Polytech.* **1966**, *10*, 183.

(31) Giori, C.; Hayes, B. T. Hydrolytic Polymerization of Caprolactam. II. Vapor−Liquid Equilibrium. *J. Polym. Sci., Polym. Chem. Ed.* **1970**, *8*, 351−358.

(32) Van Ness, H. C.; Byer, S. M.; Gibbs, R. E. Vapor−Liquid Equilibrium: Part 1. An Appraisal of Data Reduction Methods. *AIChE J.* **1973**, *19*, 238−244.

(33) Wisniak, J. A New Test for the Thermodynamic Consistency of Vapor−Liquid Equilibrium. *Ind. Eng. Chem. Res.* **1993**, *32*, 1531−1533.

(34) Prausnitz, J. M.; Lichtenthaler, R. N.; de Azevedo, E. G. *Molecular Thermodynamics of Fluid-Phase Equilibrium*, 3rd ed.; Prentice Hall: Englewood Cliffs, NJ, 1999; p 247.

(35) Herington, E. F. G. Tests for the Consistency of Experimental Isobaric Vapour-Liquid Equilibrium Data. *J. Pet. Inst.* **1951**, *37*, 457−470.

(36) Daubert, T. E.; Danner, R. P. *Physical and Thermodynamic Properties of Pure Chemicals. Data Compilation*; Hemisphere Publishing Corp.: New York, 1989; Vol. 1.

(37) Prausnitz, J. M.; Lichtenthaler, R. N.; de Azevedo, E. G. *Molecular Thermodynamics of Fluid-Phase Equilibrium*, 3rd ed.; Prentice Hall: Englewood Cliffs, NJ, 1999; p 249.

(38) Nagasubramanian, K.; Reimschuessel, H. K. Diffusion of Water and Caprolactam in Nylon-6 Melts. *J. Appl. Polym. Sci.* **1973**, *17*, 1663−1677.

(39) Nagasubramanian, K.; Reimschuessel, H. K. Caprolactam Polymerization. Polymerization in Backmix Flow Systems. *J. Appl. Polym. Sci.* **1972**, *16*, 929−934.

(40) Tirrell, M. V.; Pearson, G. H.; Weiss, R. A.; Laurence, R. L. An Analysis of Caprolactam Polymerization. *Polym. Eng. Sci.* **1975**, *15*, 386-393.

(41) Wagner, J. W.; Haylock, J. C. Control of Viscosity and Polycaproamide Degradation during Vacuum Polymerization. U.S. Patent RE28,937, 1976.

(42) Wright, W. H.; Bingham, A. J.; Fox, W. A. Method to Prepare Nylon-6 Prepolymer Providing a Final Shaped Article of Low Oligomer Content. U.S. Patent 3,813,366, 1974.

(43) Boggs, B. A.; Balint, L. J.; Ager, P. W.; Buyalos, E. J. Wiped-Wall Reactor. U.S. Patent 3,976,431, 1976.

(44) Saunders, L. V. J.; Rochell, D. Polymer Finisher. U.S. Patent 3,686,826, 1972.

(45) Whitman, W. G. The Two-Film Theory of Gas Absorption. *Chem. Metall. Eng.* **1923**, *29*, 146−148.

Received for review February 6, 2003
Revised manuscript received June 9, 2003
Accepted June 10, 2003

IE030112+